

# Loss Mechanisms Determining the Quality Factors in Quartz Tuning Forks Vibrating at the Fundamental and First Overtone Modes

Pietro Patimisco, Angelo Sampaolo, Verena Mackowiak, Hubert Rossmadl, Alex Cable,  
Frank K. Tittel, *Life Fellow, IEEE*, and Vincenzo Spagnolo 

**Abstract**—Quartz tuning forks (QTFs) are piezo-transducers that have been implemented for numerous applications, such as chemical gas sensing, atomic force microscopy, rheology, and industrial process control. The most important parameter for QTFs' sensing application is the resonance quality factor (Q-factor). An experimental investigation and theoretical analysis of the influence of QTFs' geometries on the Q-factor of the flexural fundamental and first overtone resonance modes are reported. The resonance frequencies and related Q-factors for five different QTFs have been measured. The QTF response was recorded at different air pressures to investigate the influence of the surrounding medium on the Q-factor. A data analysis demonstrated that air viscous damping is the dominant energy dissipation mechanism for both flexural modes. Thermoelastic and support losses are additional contributions that depend on the QTF geometry. A study of the QTF damping mechanism dependence upon the prong geometry is also provided.

**Index Terms**—Fundamental and overtone modes, loss mechanisms, quality factor (Q-factor), quartz tuning fork (QTF).

## I. INTRODUCTION

THE quartz tuning fork (QTF) is one of the best acoustic resonators and has the form of a two-pronged fork. It represents the central component for timing and frequency applications, due to its high resonance frequency stability and precision [1]. However, in the last few years QTFs have been implemented also for several other applications, such as atomic force microscopy (AFM) [2]–[4], near-field optical microscopy [5], quartz-enhanced photoacoustic spectroscopy (QEPAS) for gas sensing applications [6], [7], rheology [8], and gas pressure, density, and viscosity measurements [9]. When the QTF is excited at one of its flexural resonance mode or their harmonics, the two prongs oscillate in counterphase. The center of mass remains at rest, and all forces

are compensated in the support connecting the two prongs. This is in contrast with a single resonating single cantilever beam, which has an oscillating center of mass that dissipates energy. The inverse piezoelectric effect allows use of electrical excitation to both induce and detect an oscillation in a QTF. Timing applications required a QTF's geometry and crystal-cut optimized to provide a constant resonance frequency of  $2^{15}$  ( $\sim 32.7$  kHz) over a wide temperature range [1]. For different applications, such as gas sensing, AFM as well as a viscometer, accelerometer, or gyroscope, other QTFs' parameters are fundamental. For example, having a stiffness as small as possible is crucial for AFM applications [10], while for QEPAS gas sensing, the QTF resonance quality factor (Q-factor), defined as the ratio of the total input energy into the device to the energy dissipated within a vibration cycle, is the most important parameter [11]. The QEPAS sensor signal can be expressed as  $S \propto (Q \cdot P \cdot \alpha)$ , where  $Q$  is the QTF resonance Q-factor,  $\alpha$  is the gas target absorption coefficient, and  $P$  is the laser power. Furthermore, a high Q-factor also implies a small resonance bandwidth, which makes the resonator response more selective in detecting external excitations and high Q-values correspond to low dissipation losses. To realize custom QTF resonators with a high Q-factor, it is important to understand the main physical factors contributing to the energy dissipation. The main energy dissipation mechanism occurring in a vibrating prong of a QTF are damping by the surrounding fluid [12]–[14], support loss due to the interaction of the prong with its support [15], [16], and thermoelastic damping [19]. All these loss mechanisms strongly depend on prong size and the dynamics of the vibrational mode under consideration. Several theoretical models have been proposed for each loss mechanism, and their dependence on the main physical parameters has been reported. Each loss contribution is independent from the other, but all occur simultaneously for a vibrating QTF prong. To study how different loss mechanisms contribute to the complete vibrational mode resonance Q-factor, we realized and studied a set of QTFs with different prong lengths, thicknesses, and widths in an air pressure range from 20 to 760 torr. This investigation was performed for both the fundamental and first overtone in-plane flexural modes. Our analysis allows the separation of the contribution of the main loss mechanism due to air damping, and an analysis of the dependence of the other two dissipation contributions on the prong geometry, i.e., support and thermoelastic losses.

Manuscript received June 26, 2018; accepted June 29, 2018. Date of publication July 5, 2018; date of current version October 3, 2018. The work of P. Patimisco, A. Sampaolo, and V. Spagnolo was supported by Thorlabs GmbH, within PolySense, a Joint-Research Laboratory. The work of F. K. Tittel was supported by Welch Foundation under Grant R4925S. (Corresponding author: Vincenzo Spagnolo.)

P. Patimisco, A. Sampaolo, and V. Spagnolo are with the PolySense Lab, Dipartimento Interateneo di Fisica, University and Politecnico of Bari, I-70100 Bari, Italy (e-mail: vincenzoluigi.spagnolo@poliba.it).

V. Mackowiak and H. Rossmadl are with Thorlabs GmbH, 85221 Dachau, Germany.

A. Cable is with Thorlabs Inc., Newton, NJ 07860 USA.

F. K. Tittel is with the Department of Electrical and Computer Engineering, Rice University, Houston, TX 77005 USA.

Digital Object Identifier 10.1109/TUFFC.2018.2853404

## II. DAMPING MECHANISMS OF A CANTILEVER BEAM

A QTF can be treated as two identical cantilevers (prongs) coupled by a low-loss quartz bridge. Each prong can be approximated by a 2-D bar, since the crystal width is typically much smaller than the prong thickness and length. The Euler–Bernoulli beam theory describes the relationship between the deflection of the beam and its applied load and allows extraction of the discrete infinite natural resonance frequencies  $f_n$  for in-plane flexural modes given by [12]

$$f_n = \frac{\pi T}{8\sqrt{12}L^2} \sqrt{\frac{E}{\rho}} m_n^2 \quad (1)$$

where  $E = 0.72 \times 10^{11}$  N/m<sup>2</sup> is the component of the quartz Young's modulus in the vibrating plane of the QTF and  $\rho = 2650$  kg/m<sup>3</sup> denotes the quartz density,  $T$  is the prong thickness,  $L$  is the length, and  $m_n$  is the mode number. The lowest resonance mode is usually referred to as the fundamental mode ( $m_0 = 1.194$ ), while subsequent ones are called overtone modes ( $m_1 = 2.998$  for the first overtone mode). High  $Q$ -factors for a vibrational resonance mode result in low dissipation losses for the vibrating prongs and consequently a sharp frequency response. The main loss mechanisms in a QTF are due to: 1) air damping, related to the transfer of energy and momentum from the QTF prongs to the surrounding medium; 2) support loss, related to transfer of mechanical energy from the vibrating prong to the support; and 3) thermoelastic damping, related to coupling between the strain field and the temperature field inside the QTF. Each resonance mode is characterized by a different vibration profile along the prongs axis with antinode points that identify the position of maximum vibration amplitudes along the prong. In other words, each vibrational mode is expected to exhibit a different  $Q$ -factor, because loss mechanisms are also dependent on the related vibrational dynamics [20]–[23].

When a QTF vibrating prong is immersed in air, a drag force is exerted on it. In the viscous region, the medium acts as a viscous fluid, and the drag force is calculated using fluid mechanics. With the assumption that the length  $L$  of the QTF prong is much greater than its thickness  $T$  and crystal width  $w$ , Hosaka *et al.* [12] derived a formulation of the  $Q$ -factor related to fluid damping ( $Q_{\text{air}}$ )

$$Q_{\text{air}} = \frac{4\pi\rho T w^2 f_n}{3\pi\mu w + \frac{3}{4}\pi w^2 \sqrt{4\pi\rho_{\text{air}}\mu f_n}} \quad (2)$$

where  $\rho_{\text{air}}$  is the air density and  $\mu$  is the viscosity. In Fig. 1(a),  $Q_{\text{air}}$  is plotted as a function of the pressure considering a QTF having  $L = 17$  mm,  $T = 1.0$  mm, and  $w = 0.25$  mm, for both the fundamental and the first overtone modes ( $\mu = 1.81 \times 10^{-5}$  kg/m · s).  $\rho_{\text{air}} = MP/R\Theta$  is estimated by using the ideal gas law, where  $M = 28.964$  kg/mol is the molar mass,  $R = 62.3637$  m<sup>3</sup> · torr/k · mol is the gas constant, and  $\Theta$  (in K) is the prong temperature. In both cases,  $Q_{\text{air}}$  decreases very rapidly when the pressure increases from 25 to 150 torr. At higher pressures,  $Q_{\text{air}}$  levels off and becomes quasi-asymptotic at atmospheric pressure. The air damping mechanisms are strongly reduced for higher order vibrational modes. By combining (1) and (2), an explicit dependence of

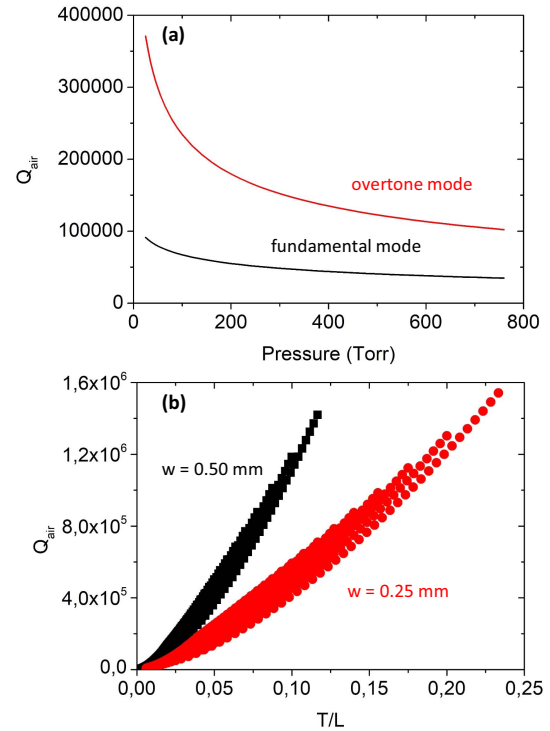


Fig. 1. (a)  $Q_{\text{air}}$  plotted as a function of the gas pressure for a QTF with a prong length and width of 17.0 and 1.0 mm, respectively, and a crystal thickness of 0.25 mm for the fundamental (black solid curve) and the first overtone (red solid curve) mode. (b)  $Q_{\text{air}}$  plotted as a function of the ratio between the prong thickness  $T$  and its length  $L$  for a crystal thickness of  $w = 0.25$  mm (●) and  $w = 0.5$  mm (■) at an air pressure of 50 torr.

$Q_{\text{air}}$  can be derived as a function of the prong size. In Fig. 1(b),  $Q_{\text{air}}$  is plotted as a function on the ratio  $T/L$ , in which  $L$  ranges from 3 to 17 mm and  $0.2 < T < 1.4$  mm, for  $w = 0.25$  mm and  $w = 0.5$  mm. The data were simulated at an air pressure of 50 torr. For a fixed pressure and crystal width, a quasi-linear dependence of  $Q_{\text{air}}$  on the ratio  $T/L$  is observed. The guideline that emerges from this model is that to reduce viscous losses; the  $T/L$  ratio must be kept high. In addition, the lower the crystal thickness, the higher will be the air damping losses.

The simplest model to study support losses was developed by Hao *et al.* [17], in which the prong is supposed to be a rectangular cross-sectional resonator, attached monolithically to a larger support with the same thickness as that of the prong. The crystal thickness  $w$  is assumed to be much smaller than the elastic wavelength  $\lambda$  of the propagating waves. The closed-form expression for the  $Q$ -factor related to the support loss in a clamped-free cantilever was expressed as

$$Q_{\text{supp}} = A_n \frac{L^3}{T^3} \quad (3)$$

with  $A_n$  coefficients depending on the resonance mode number and the prong material. Hao *et al.* [17] estimated  $A_0 = 2.081$  for the fundamental mode and  $A_1 = 0.173$  for the first overtone mode.

Thermoelastic dissipation is an intrinsic structural dissipation mechanism of the oscillating elements, which can be expressed using a modeling approach proposed by Zener [19].

TABLE I

DIMENSIONS OF THE CUSTOM TUNING FORKS:  $L$  (PRONG LENGTH),  $T$  (PRONG THICKNESS), AND  $w$  (QUARTZ CRYSTAL THICKNESS)

QTF	Prong length $L$ (mm)	Crystal width $w$ (mm)	Prong thickness $T$ (mm)
#1	3.5	0.25	0.2
#2	10.0	0.25	0.9
#3	10.0	0.50	1.0
#4	11.0	0.25	0.5
#5	17.0	0.25	1.0

The  $Q$ -factor  $Q_{\text{TED}}$  related to thermoelastic loss for an isotropic homogeneous beam can be expressed as

$$Q_{\text{TED}} = \frac{\rho c_T}{E\beta^2\Theta} \cdot \frac{1 + \left(\frac{2c_T f_n \rho T^2}{\pi \lambda_T}\right)^2}{\frac{2c_T f_n \rho T^2}{\pi \lambda_T}} \approx \frac{2(\rho c_T)^2 f_n T^2}{E\beta^2\Theta \pi \lambda_T} \propto \frac{T^3}{L^2} \quad (4)$$

where  $\lambda_T$ ,  $c_T$ , and  $\beta$  are the thermal conductivity, the heat capacity per unit mass, and the thermal expansion of the prong, respectively. This expression is based on the assumption of an isotropic beam. By combining (1) and (4), in a first approximation,  $Q_{\text{TED}}$  scales with prong size as  $T^3/L^2$ .

### III. EXPERIMENTAL MEASUREMENTS

To investigate the dependence of loss mechanisms on the prong size of QTFs vibrating at the fundamental and overtone modes, a set of five different QTFs was designed and then realized. The geometrical properties of the QTFs are listed in Table I.

The QTFs were realized starting from a  $z$ -cut quartz wafer with a  $2^\circ$  rotation along the  $x$ -axis, since this crystal-cut provides stable flexural vibrational modes frequencies at room temperature. Furthermore, the  $z$ -cut is the crystal-cut typically used for QTFs operating at low frequencies (up to 50 kHz). The quartz wafers were etched. A 3-D crystal structure is generated by chemical etching in a saturated aqueous solution of ammonium bifluoride. The temperature of the chemical etching solution was monitored directly by a temperature controller and kept at a constant  $52^\circ\text{C}$ . This temperature was chosen because it allows chemical etching in a reasonable amount of time while also permitting adequate control of frequency by adjusting the etching time. Constant agitation was provided by a motor-driven rotary propeller. Electrodes, consisting of chromium ( $50\text{ \AA}$  thick) and gold ( $250\text{ \AA}$  thick) patterns, are applied photolithographically by means of shadow masks defined on both sides of the wafer. The gap between the center and side electrodes is  $50\text{ }\mu\text{m}$ . A schematic of the investigated QTF set is shown in Fig. 2.

The electrode layout was not only designed to enhance the fundamental flexural mode but also allowing the excitation of the first overtone mode. Due to the piezoelectricity of quartz, when a stress is applied to a QTF prong, a displacement of charge and a net electric field are induced. The effect is reversible and when a voltage is applied to a piezoelectric

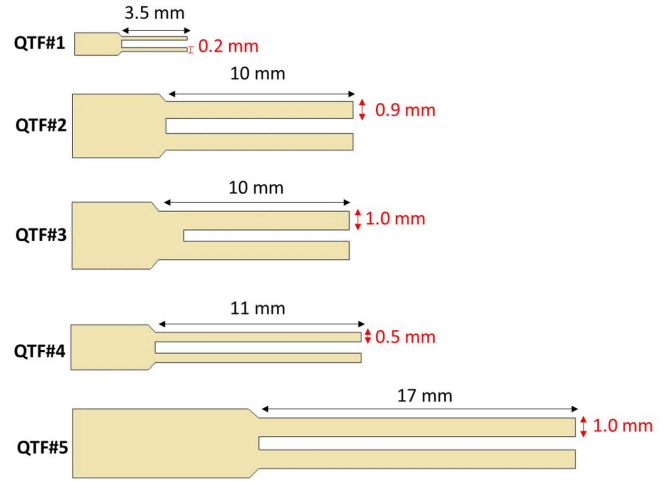


Fig. 2. Schematic of the investigated QTFs labeled as in Table I.

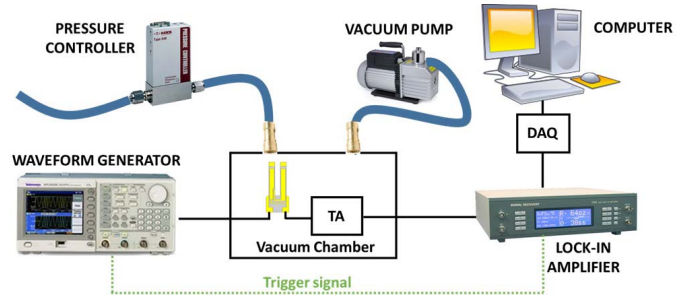


Fig. 3. Schematic of the experimental setup. TA: transimpedance amplifier and DAQ: data acquisition card.

material, it is accompanied by a strain. Hence, the QTF response can be obtained by exciting the resonator electrically. The experimental setup used to characterize custom QTFs via electrical excitation is schematically depicted in Fig. 3. A waveform generator, Tektronix AFG 3102, generates a sinusoidal voltage excitation, which results in a piezoelectric charge distribution across the QTF prongs.

This piezoelectric current is then converted to an output voltage by means of a custom-made transimpedance amplifier (TA) amplifier with a feedback resistor of  $10\text{ M}\Omega$  and gain factor of  $\sim 30$ . The TA output voltage is fed to a commercial lock-in amplifier (7265 dual-phase DSP lock-in amplifier from signal recovery), which demodulates the signal at the same frequency of the waveform generator. The demodulated signal is then sent to a data acquisition (DAQ) card (NI USB 6009), which is interfaced with a PC for data analysis. The QTF was mounted in a vacuum chamber. The vacuum chamber was connected with a gas line that included a pressure controller and an oil-free pump. In this way, it was possible to select and fix the air pressure in the vacuum chamber in the range between 20 and 760 torr.

### IV. MEASUREMENTS OF RESONANCE FREQUENCIES AND QUALITY FACTORS

The Euler–Bernoulli equation can be used to predict the theoretical frequencies for the fundamental and the

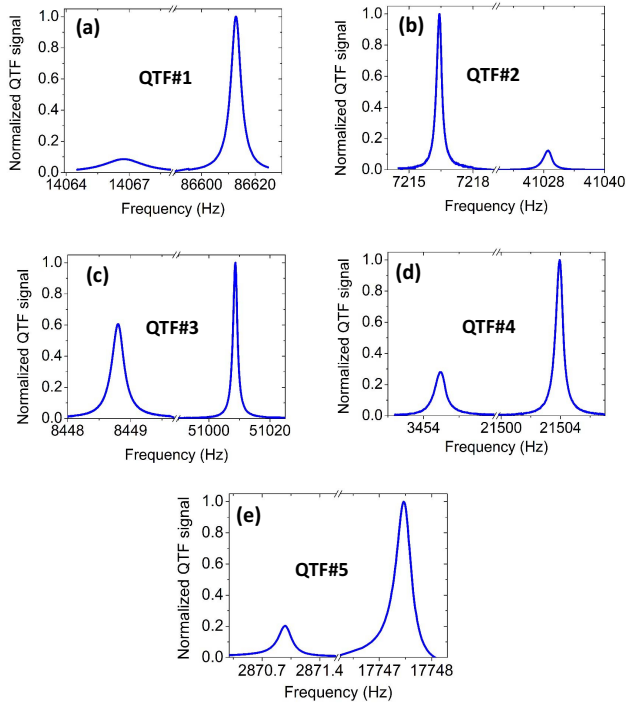


Fig. 4. QTFs' resonance curves measured at a pressure of 50 torr in standard air for (a) QTF#1, (b) QTF#2, (c) QTF#3, (d) QTF#4, and (e) QTF#5, for the fundamental and first overtone modes. In each graph, curves are normalized to the related highest signal value.

overtone modes. The actual values can be determined by performing a wide frequency range, using a custom-made LabVIEW-based software to vary step-by-step the frequency of the waveform generator (with an excitation peak-to-peak voltage of 0.5 mV) and acquire the lock-in output via the DAQ. As an example, Fig. 4 shows the spectral response of the QTFs at 50 torr. Once identified the center value, a well-resolved resonance curve is obtained by applying a short frequency ramp (few millihertz) around the peak. For each QTF, the fundamental and the overtone modes exhibit different peak values. The peak value is inversely proportional to the electrical resistance of the QTF, which is in turn inversely proportional to the  $Q$ -factor. The QTFs' electrical resistance values depend upon the prongs' geometry and resonance mode order [24]. Each spectral response was fitted by using a Lorentzian function to determine the resonance frequency, i.e., the peak value of the Lorentzian fit function and the full-width-half-maximum (FWHM) [25]. In Table II, the extracted values for the resonance frequencies  $f_0$  (fundamental mode) and  $f_1$  (first overtone mode) at 50 torr are reported.

The FWHM was used to determine the  $Q$ -factor as  $Q = f/\text{FWHM}$  for the fundamental and overtone modes. Fig. 5 depicts the extracted  $Q$ -factor values for the investigated set of QTFs plotted as a function of the air pressure for both fundamental and first overtone modes.

Apart from main loss mechanisms described in the previous paragraph, any asymmetry between prongs geometry results in an additional damping mechanism for the vibrating prong. The influence of prongs' asymmetries on the overall QTF  $Q$ -factor

TABLE II  
RESONANCE FREQUENCIES OF THE FUNDAMENTAL MODE ( $f_0$ ) AND THE FIRST OVERTONE MODE ( $f_1$ ) MEASURED AT 50 TORR OF AIR PRESSURE

QTF	$f_0$ (Hz)	$f_1$ (Hz)
#1	14068.14	86612.38
#2	7216.41	41028.76
#3	8448.80	51008.62
#4	3454.27	21503.81
#5	2870.98	17747.47

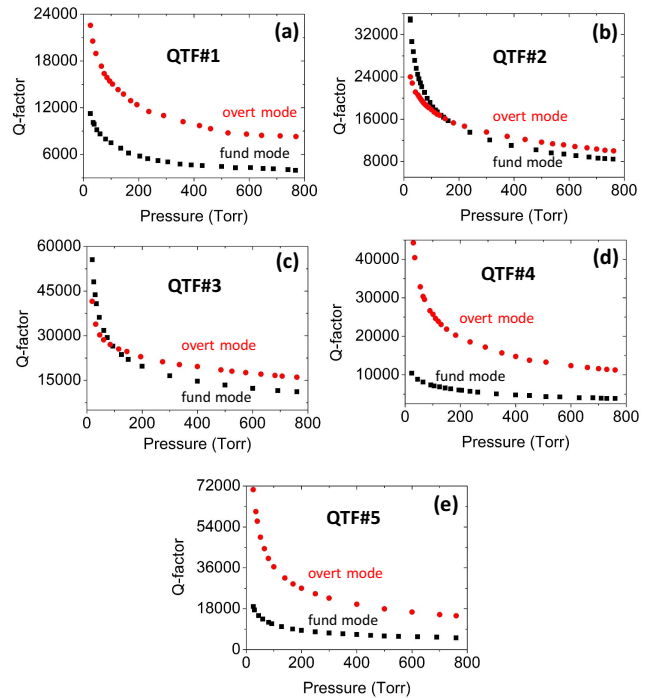


Fig. 5.  $Q$ -factors measured as a function of the air pressure for the flexural fundamental (■) and overtone (●) vibrational resonance modes, for (a) QTF#1, (b) QTF#2, (c) QTF#3, (d) QTF#4, and (e) QTF#5.

has been reported in several publications using the classical mechanical models [26], [27]. For a standard 32.7-kHz QTF ( $L = 3.5$  mm,  $T = 0.3$  mm, and  $w = 0.3$  mm), a prong symmetry breaking caused by a mass difference within 0.3% produces a decrease of the  $Q$ -factor of less than 10% [27]. For QTFs investigated in this work, such a fractional mass difference corresponds to a prong size variation of few micrometers for the shortest dimension ( $T$  for the investigated QTFs), assuming that the crystal width is not affected by the QTFs' fabrication process. To experimentally evaluate the influence of the prongs size asymmetry on the overall  $Q$ -factor, we performed a statistical study by testing different QTF samples having the same geometry and belonging to different crystal benches, with the same experimental conditions. All the QTF samples showed  $Q$ -factor values differing by less than 10%. This confirms that the QTFs' fabrication process does not produce asymmetries in the prongs geometry that can affect the QTF  $Q$ -factor.

The dependence of the measured  $Q$ -factors on air pressure follows the trend of  $Q_{\text{air}}$  reported in Fig. 1(a), suggesting that the dominant loss mechanism is air damping for both modes. The air damping dependence on the prong size can also be investigated by comparing QTFs differing only in  $T$  or  $L$ .

QTF#2 and QTF#4 share almost the same prong length ( $L = 10$  mm and  $L = 11$  mm for QTF#2 and QTF#4, respectively) and the crystal thickness ( $w = 0.25$  mm) but substantially differ in the prong thickness ( $T = 0.9$  mm and  $T = 0.5$  mm for QTF#2 and QTF#4, respectively). According to Fig. 1(b), a reduction of the prong width corresponds to an increase of the air damping mechanisms. Indeed, at atmospheric pressure, the fundamental mode of QTF#2 exhibits a  $Q$ -factor ( $Q = 8420$ ), 2.2 higher than that measured for the QTF#4 ( $Q = 3870$ ). Similarly, a reduction of the prong length causes an increase of the air damping mechanisms, when other prong sizes are equal. This statement has been verified by comparing QTF#2 ( $L = 10$  mm,  $w = 0.25$ , and  $T = 0.9$  mm) and QTF#5 ( $L = 17$  mm,  $w = 0.25$ , and  $T = 1.0$  mm), having almost the same  $w$  and  $T$  but differing in  $L$ . At atmospheric pressure, the fundamental mode  $Q$ -factor of QTF#5 is 5210, which is almost  $1.6\times$  lower than that measured for the QTF#2. For the overtone modes, the air damping mechanisms are reduced [see Fig. 1(a)] and support losses start to dominate. Support losses strongly depend on the prong geometrical factor  $L/T$  [see (3)]. In the investigated set of QTFs, the highest  $L/T$  ratios are 22, 17.5, and 17 calculated for QTF#4, QTF#1, and QTF#5, respectively. At atmospheric pressure, for these QTFs the  $Q$ -factor for the first overtone modes result in about  $3\times$  higher with respect to the  $Q$ -factor measured for the fundamental modes. Conversely, for QTF#2 and QTF#3, only a slight increase of  $Q$ -factor is observed ( $L/T = 11.1$  and  $10.0$  for QTF#2 and QTF#3, respectively). Since the dissipation mechanisms are assumed independent of each other and the resonator  $Q$ -factor is proportional to the inverse of total energy dissipated, the overall  $Q$ -factor can be represented as a reciprocal sum of independent dissipative contributions

$$\frac{1}{Q(P)} = \frac{1}{Q_{\text{air}}(P)} + \frac{1}{Q_{\text{sup}}} + \frac{1}{Q_{\text{TED}}}. \quad (5)$$

Thermoelastic and support losses are assumed to be independent to the air pressure [17]–[19], and therefore, it is possible to define  $Q(0)$  as

$$\frac{1}{Q(0)} = \frac{1}{Q_{\text{sup}}} + \frac{1}{Q_{\text{TED}}} \quad (6)$$

where  $Q_{\text{air}}$  in (2) can be expressed as a function of gas pressure by using the general gas law

$$Q_{\text{air}}(P) = \frac{a}{b + c\sqrt{P}} \quad (7)$$

where  $a = 4\pi\rho Twf_n$ ,  $b = 3\pi\mu$ , and  $c = 0.75 \cdot \pi\mu w (4\pi Mf_n\mu/N_A k_B\Theta)^{1/2}$ , since  $\rho_{\text{air}} = MP/N_A k_B\Theta$ , where  $M$  is the molar mass of air,  $N_A$  is Avogadro's number, and  $k_B$  is Boltzmann's constant. As defined,  $Q(0)$  does not include the pressure-independent contribution derived from Hosaka's model [12]. By combining (5)–(7), the overall  $Q$ -factor can

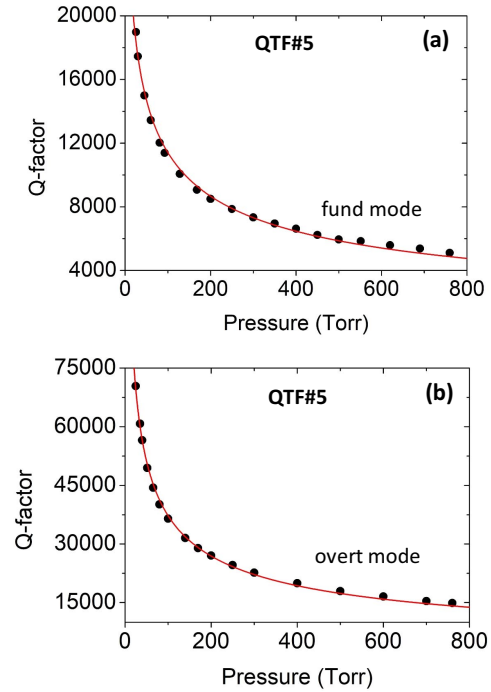


Fig. 6. Experimental  $Q$ -factor values ( $\bullet$ ) as a function of the air pressure together with the best fit obtained by using (8) when QTF#5 oscillates at the (a) fundamental and (b) first overtone modes.

be rewritten as

$$Q(P) = \frac{1}{A + B\sqrt{P}} \quad (8)$$

where  $A = 1/Q(0) + b/a$  and  $B = c/a$ . This equation was used to fit the experimental data reported in Fig. 5, both for the fundamental and overtone modes. As a representative, the experimental data and the best fit obtained by using (8) for QTF#5 are reported in Fig. 6 for the fundamental and first overtone modes.

The pressure-independent  $Q$ -factor contribution  $Q(0)$  can be extracted by subtracting  $b/a$  from the fitting parameter  $A$ , leading to  $1/Q(0) = A - b/a$ . Hosaka's model [12] was used to calculate the ratio  $b/a$  in order to estimate  $Q(0)$ . In Table III,  $A$  and  $B$  values extracted from the fit together with  $Q(0)$  values for the fundamental and overtone modes are listed for all the investigated QTFs.

Each contribution to  $Q(0)$ ,  $Q_{\text{TED}}$ , and  $Q_{\text{sup}}$  can be related with the geometrical properties of resonator:  $Q_{\text{sup}} \propto L^3/T^3$ , while  $Q_{\text{TED}} \propto T^3/L^2$ . With the analysis presented in this work, it is not possible to separate the two contributions of  $Q(0)$ . However, it is feasible to investigate the dependence of  $Q(0)$  values from the geometrical parameters of the QTF prong, since  $Q_{\text{sup}}$  and  $Q_{\text{TED}}$  show the opposite behaviors with the prong sizes.

Fig. 7(a) shows a clear linear dependence of  $Q(0)$  values on  $T^3/L^2$  ratios, which proves that the relevant dissipation mechanism at the fundamental mode is related to the thermoelastic losses and support losses can be neglected.

This agrees with the results obtained in [20] in which the support losses were negligible for QTFs vibrating at the

TABLE III

A AND B FITTING PARAMETERS OBTAINED BY USING (8), CALCULATED BY USING (2), (7), AND (8), AND  $Q(0)$  VALUES FOR THE FUNDAMENTAL AND THE FIRST OVERTONE MODES OF THE QTF SET INVESTIGATED IN THIS WORK

QTF	Fundamental mode			Overtone mode		
	A	B	Q(0)	A	B	Q(0)
	$\cdot 10^{-6}$	$\cdot 10^{-6} \text{ torr}^{-0.5}$	$\cdot 10^3$	$\cdot 10^{-6}$	$\cdot 10^{-6} \text{ torr}^{-0.5}$	$\cdot 10^3$
#1	53.6	7.8	21.6	28.8	3.53	36.2
#2	8.9	4.35	174	31.1	2.49	32.6
#3	2.6	3.6	184	20	1.6	51.1
#4	62.6	7.37	19.7	6.7	3.15	209
#5	20.3	6.9	75.6	1.7	2.52	100

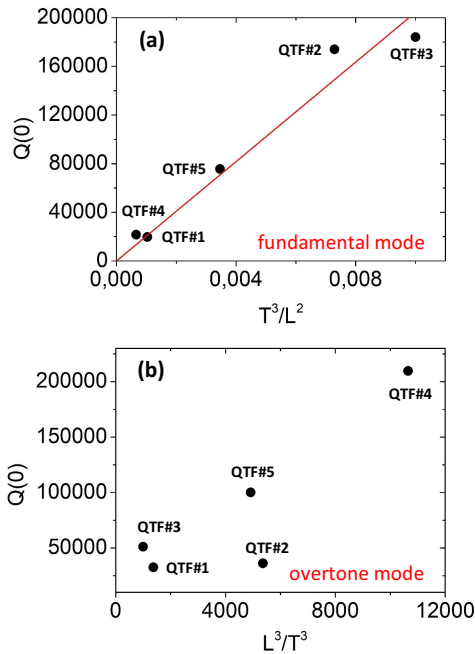


Fig. 7.  $Q(0)$  values ( $\bullet$ ) plotted as a function of the ratio  $T^3/L^2$  for the (a) fundamental mode and as a function of  $L^3/T^3$  for the (b) first overtone mode. Red solid line: best linear fit.

fundamental mode, since an empirical correlation between the  $Q$ -factor and  $Tw/L$  parameter at a pressure as low as 50 torr was observed (see Fig. 1). Conversely, for the overtone mode,  $Q(0)$  values are positively correlated with  $L^3/T^3$ , as shown in Fig. 7(b), indicating that the support losses contribution is not negligible for the overtone modes, even if a contribution due to thermoelastic damping is assumed to be present. This result agrees with the theoretical model proposed by Hao [see (3)] that predicts an increase of the support losses of a factor of  $A_0/A_1 \sim 12$  when transitioning from the fundamental mode to the overtone mode.

## V. CONCLUSION

In this work, the dependence of QTFs' fundamental and first overtone flexural resonance modes  $Q$ -factors on the dimensions of the prongs was investigated. This analysis

was performed employing an experimental setup allowing the acquisition of the spectral response of an electrically excited tuning fork in the pressure range between 20 and 760 torr. A set of five tuning QTFs differing in prong sizes was realized and tested. All QTFs were excited both at the fundamental and the first overtone in-plane flexural modes resonance frequencies. The  $Q$ -factor significantly decreases when the pressure increases from 20 torr to atmospheric pressure. This behavior suggested that a QTF mainly loses energy via the interaction with the surround viscous medium. The air damping mechanism was modeled by using an analytical expression derived by Kokubun *et al.* [13] and found to be in excellent agreement with the experimental data. Two other mechanisms of losses, pressure independent and strongly dependent on the prong geometry, were considered: support and thermoelastic losses. The analysis proposed does not allow us to separate these two contributions. However, the two mechanisms showed the opposite trends with the prong geometry: the support loss contribution varies as  $L^3/T^3$  while thermoelastic losses scale as  $T^3/L^2$ . By using such dependences, our results showed that support losses can be neglected at the fundamental mode, while they became relevant for the overtone mode. In particular, air damping is reduced at the first overtone mode with respect to the fundamental mode, and support losses become the relevant mechanism of energy dissipation at low pressures. All these results represent a guideline for the design of QTFs optimized for QEPAS applications. Typically, for QEPAS gas sensing the fundamental flexural resonance mode is exploited for optoacoustic detection. However, recently QEPAS sensors implementing QTF operating at the first overtone flexural mode have been demonstrated [20], [21], [28], [29]. Therefore, by an appropriate design of the QTF prongs geometry, it is possible to realize QTFs having high  $Q$ -factors selectively for the fundamental or the first overtone mode resonances.

Finally, it is worth noting that although the dependence of support losses on the prong geometry was verified, the analytical models proposed in the literature did not allow an exact calculation of the contributions to the overall  $Q$ -factor due to support and thermoelastic losses. Hence, this study confirmed the limit of the analytical models. Other computational methods (for example, finite-element method analysis) are mandatory for a precise prediction of the overall  $Q$ -factor of a damped QTF.

## REFERENCES

- [1] J.-M. Friedt and É. Carry, "Introduction to the quartz tuning fork," *Amer. J. Phys.*, vol. 75, no. 5, pp. 415–422, 2007.
- [2] R. D. Grober *et al.*, "Fundamental limits to force detection using quartz tuning forks," *Rev. Sci. Instrum.*, vol. 71, no. 7, pp. 2776–2780, 2000.
- [3] F. J. Giessibl, "Atomic resolution on Si(111)-(7 $\times$ 7) by noncontact atomic force microscopy with a force sensor based on a quartz tuning fork," *Appl. Phys. Lett.*, vol. 76, no. 11, pp. 1470–1472, 2000.
- [4] H. Göttlich, R. W. Stark, J. D. Pedarnig, and W. M. Heckl, "Noncontact scanning force microscopy based on a modified tuning fork sensor," *Rev. Sci. Instrum.*, vol. 71, no. 8, pp. 3104–3107, 2000.
- [5] F. J. Giessibl, "High-speed force sensor for force microscopy and profilometry utilizing a quartz tuning fork," *Appl. Phys. Lett.*, vol. 73, no. 26, pp. 3956–3958, 1998.

- [6] A. A. Kosterev, F. K. Tittel, D. Serebryakov, A. L. Malinovsky, and I. A. Morozov, "Applications of quartz tuning forks in spectroscopic gas sensing," *Rev. Sci. Instrum.*, vol. 76, no. 4, pp. 043105-1–043105-9, 2005.
- [7] P. Patimisco, A. Sampaolo, L. Dong, F. K. Tittel, and V. Spagnolo, "Recent advances in quartz enhanced photoacoustic sensing," *Appl. Phys. Rev.*, vol. 5, no. 1, pp. 011106-1–011106-19, 2018.
- [8] M. Gonzalez, H. R. Seren, G. Ham, E. Buzi, G. Bernero, and M. Deffenbaugh, "Viscosity and density measurements using mechanical oscillators in oil and gas applications," *IEEE Trans. Instrum. Meas.*, vol. 67, no. 4, pp. 804–810, Apr. 2018.
- [9] D. Garg, V. B. Efimov, M. Giltrow, P. V. E. McClintock, L. Skrbek, and W. F. Vinen, "Behavior of quartz forks oscillating in isotopically pure  $^4\text{He}$  in the  $T \rightarrow 0$  limit," *Phys. Rev. B, Condens. Matter*, vol. 85, pp. 144518-1–144518-13, 2012.
- [10] B. Walter, E. Mairiaux, and M. Faucher, "Atomic force microscope based on vertical silicon probes," *Appl. Phys. Lett.*, vol. 100, no. 24, pp. 243101-1–243101-4, 2017.
- [11] M. Christen, "Air and gas damping of quartz tuning forks," *Sens. Actuators*, vol. 4, pp. 555–564, 1983.
- [12] H. Hosaka, K. Itao, and S. Kuroda, "Damping characteristics of beam-shaped micro-oscillators," *Sens. Actuators A, Phys.*, vol. 49, pp. 87–95, Jun. 1995.
- [13] K. Kokubun, M. Hirata, H. Murakami, Y. Toda, and M. Ono, "A bending and stretching mode crystal oscillator as a friction vacuum gauge," *Vacuum*, vol. 34, nos. 8–9, pp. 731–735, 1984.
- [14] F. R. Blom, S. Bouwstra, M. Elwenspoek, and J. H. J. Fluitman, "Dependence of the quality factor of micromachined silicon beam resonators on pressure and geometry," *J. Vac. Sci. Technol. B, Microelectron. Process. Phenom.*, vol. 10, no. 1, pp. 19–26, 1992.
- [15] Y. Jimbo and K. Itao, "Energy loss of a cantilever vibrator," *J. Horol. Inst. Jpn.*, vol. 47, pp. 1–15, Jan. 1968.
- [16] D. M. Photiadis and J. A. Judge, "Attachment losses of high *Q* oscillators," *Appl. Phys. Lett.*, vol. 85, no. 3, pp. 482–484, 2005.
- [17] Z. Hao, A. Erbil, and F. Ayazi, "An analytical model for support loss in micromachined beam resonators with in-plane flexural vibrations," *Sens. Actuators A, Phys.*, vol. 109, pp. 156–164, Dec. 2003.
- [18] J. A. Judge, D. M. Photiadis, J. F. Vignola, B. H. Houston, and J. Jarzynski, "Attachment loss of micromechanical and nanomechanical resonators in the limits of thick and thin support structures," *J. Appl. Phys.*, vol. 101, pp. 013521-1–013521-11, 2007.
- [19] C. Zener, "Internal friction in solids II. General theory of thermoelastic internal friction," *Phys. Rev.*, vol. 53, pp. 90–99, Jan. 1938.
- [20] A. Sampaolo *et al.*, "Quartz-enhanced photoacoustic spectroscopy exploiting tuning fork overtone modes," *Appl. Phys. Lett.*, vol. 107, no. 23, pp. 231102-1–231102-4, 2015.
- [21] P. Patimisco, A. Sampaolo, H. Zheng, L. Dong, F. K. Tittel, and V. Spagnolo, "Quartz-enhanced photoacoustic spectrophones exploiting custom tuning forks: A review," *Adv. Phys. X*, vol. 2, no. 1, pp. 169–187, 2016.
- [22] K. Kokubun, M. Hirata, M. Ono, H. Murakami, and Y. Toda, "Frequency dependence of a quartz oscillator on gas pressure," *J. Vac. Sci. Technol. A, Vac. Surf. Films*, vol. 3, no. 6, pp. 2184–2187, 1985.
- [23] W. E. Newell, "Miniaturization of tuning forks," *Science*, vol. 161, no. 3848, pp. 1320–1326, 1968.
- [24] M. Hirata, K. Kokubun, M. Ono, and K. Nakayama, "Size effect of a quartz oscillator on its characteristics as a friction vacuum gauge," *J. Vac. Sci. Technol. A, Vac. Surf. Films*, vol. 3, no. 3, pp. 1742–1745, 1985.
- [25] D. I. Bradley *et al.*, "Stability of flow and the transition to turbulence around a quartz tuning fork in superfluid  $^4\text{He}$  at very low temperatures," *Phys. Rev. B, Condens. Matter*, vol. 89, pp. 214503-1–214503-9, Jun. 2014.
- [26] A. Castellanos-Gomez, N. Agrait, and G. Rubio-Bollinger, "Dynamics of quartz tuning fork force sensors used in scanning probe microscopy," *Nanotechnology*, vol. 20, no. 21, p. 215502, 2009.
- [27] J. Rycken, T. Ihn, P. Studerus, A. Herrmann, and K. Ensslin, "A low-temperature dynamic mode scanning force microscope operating in high magnetic fields," *Rev. Sci. Instrum.*, vol. 70, no. 6, pp. 2765–2768, 1999.
- [28] H. Zheng *et al.*, "Overtone resonance enhanced single-tube on-beam quartz enhanced photoacoustic spectrophone," *Appl. Phys. Lett.*, vol. 109, no. 11, pp. 111103-1–111103-5, 2016.
- [29] H. Wu *et al.*, "Simultaneous dual-gas QEPAS detection based on a fundamental and overtone combined vibration of quartz tuning fork," *Appl. Phys. Lett.*, vol. 110, no. 12, pp. 121104-1–121104-4, 2017.



**Pietro Patimisco** received the master's (*cum laude*) and Ph.D. degrees in physics from the University of Bari, Bari, Italy, in 2009 and 2013, respectively.

He was a Visiting Scientist with the Laser Science Group, Rice University, Houston, TX, USA, in 2013 and 2014. Since 2013, he has been a Post-Doctoral Research Associate with the University of Bari. His scientific activity addressed both microprobe optical characterization of semiconductor optoelectronic devices and photoacoustic gas sensors. His research interests included the study and applications of trace-gas sensors, such as quartz-enhanced photoacoustic spectroscopy and cavity-enhanced absorption spectroscopy in the mid infrared and terahertz spectral region, leading to several publications, including a cover paper in *Applied Physics Letter* in the July 2013 issue.



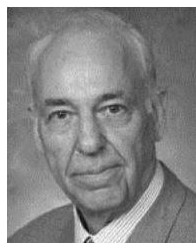
**Angelo Sampaolo** received the master's and Ph.D. degrees in physics from the University of Bari, Bari, Italy, in 2013 and 2017, respectively.

He was a Visiting Researcher with the Laser Science Group, Rice University, Houston, TX, USA, in 2016 and 2017. Since 2017, he has been a Post-Doctoral Research Associate with the University of Bari. His research interests included the study of the thermal properties of heterostructured devices via Raman spectroscopy. Most recently, his research interests include the development of innovative techniques in trace-gas sensing, based on quartz-enhanced photoacoustic spectroscopy and covering the full spectral range from near-infrared to terahertz. His achieved results have been acknowledged by a cover paper in *Applied Physics Letter* in the July 2013 issue.

**Verena Mackowiak**, photograph and biography not available at the time of publication.

**Hubert Rossmadl**, photograph and biography not available at the time of publication.

**Alex Cable**, photograph and biography not available at the time of publication.



**Frank K. Tittel** (SM'72–F'86–LF'03) received the bachelor's, master's, and Ph.D. degrees in physics from the University of Oxford, Oxford, U.K., in 1955 and 1959, respectively.

From 1959 to 1967, he was a Research Physicist with the General Electric Research and Development Center, Schenectady, NY, USA. Since 1967, he has been a Faculty Member with the Department of Electrical and Computer Engineering and Biomedical Engineering, Rice University, Houston, TX, USA, where he is currently an Endowed Chair Professor. His current research interests include the various aspects of quantum electronics, in particular, laser spectroscopy and laser applications in environmental monitoring, atmospheric chemistry, industrial process control, and medical diagnostics.

Dr. Tittel is a Fellow of the Optical Society of America, the American Physical Society, and SPIE.



**Vincenzo Spagnolo** received the Ph.D. degree in physics from the University of Bari, Bari, Italy, in 1994.

From 1997 to 1999, he was a Researcher with the National Institute of the Physics of Matter, Bari. Since 2004, he has been with the Technical University of Bari, formerly as Assistant Professor and, starting from 2015, as Associate Professor of physics. He is currently the Director of the Joint-Research Lab Polysense, created by the Technical University of Bari and Thorlabs GmbH, Dachau, Germany. He has authored over 160 publications and two filed patents. He has given over 40 invited presentations at international conferences and workshops. His research interests include photoacoustic gas sensing and spectroscopic techniques for real-time device monitoring.

Dr. Spagnolo is a Senior Member of SPIE and OSA.